THE JOURNAL OF PHYSICAL CHEMISTRY C

ARTICLE

pubs.acs.org/JPCC

Pore Size Effects on the Sorption of Supercritical CO_2 in Mesoporous CPG-10 Silica

Gernot Rother,*,† Elizabeth G. Krukowski,‡ Dirk Wallacher,§ Nico Grimm,§ Robert J. Bodnar,‡ and David R. Cole∥

†Geochemistry and Interfacial Science Group, Chemical Sciences Division, Oak Ridge National Laboratory, Oak Ridge, Tennessee 37831-6110, United States

‡Fluids Research Laboratory, Virginia Tech, Blacksburg, Virginia 24061, United States

§Helmholtz-Zentrum Berlin fur Materialien und Energie GmbH, Hahn-Meitner Platz 1, D-14109 Berlin, Germany

∥School of Earth Sciences, Ohio State University, 125 South Oval Mall, Columbus, Ohio 43210, United States

ABSTRACT: Excess sorption isotherms of supercritical carbon dioxide in mesoporous CPG-10 silica glasses with nominal pore sizes of 7.5 and 35 nm were measured gravimetrically at 35 and 50 °C and pressures of 0−200 bar. Formation of broad maxima in the excess sorption was observed at fluid densities below the bulk critical density. Positive values of excess sorption were measured at bulk densities below 0.7 g/cm^3, i.e., the interfacial fluid is denser than the bulk fluid at low pressures. Zero and negative values were obtained at higher densities, i.e., the adsorbed fluid becomes equal to and eventually less dense than the corresponding bulk fluid. Pronounced confinement effects on sorption behavior have been found and further analyzed by normalizing the excess sorption to the adsorbent surface area and pore volume, yielding new insight into supercritical fluid adsorption in this range of pore sizes and P, T conditions. If normalized to the specific surface area, the excess sorption is higher for the 35 nm pore size material, but the pore volume normalized excess sorption is higher for the 7.5 nm pore size material. With increasing pore width, the excess sorption peak position shifts to higher pressure. Both CPG-10 materials exhibit regions of constant mean pore fluid density as a function of bulk CO_2 density at 35 °C but not at 50 °C. This region is located between the excess sorption peak maximum and the adsorption/depletion transition point. Applied to the situation of CO_2 sequestration in dry sandstone formations, the results of this study indicate that carbon storage capacity is enhanced by sorption effects, particularly at low temperature and in narrow pores with high surface to volume ratios.

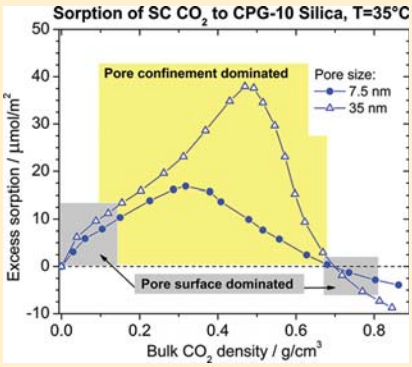

1. INTRODUCTION

The properties of fluids in confined geometries (pores and fractures) differ from their bulk behavior, owing to the effects of large internal surfaces and geometrical confinement.[1] Phase transitions (i.e., freezing and capillary condensation), sorption and wetting, and dynamical properties, including diffusion and relaxation, of fluids may be modified in small pores, with the largest changes observed for pores ranging in size from <2 to 50 nm, the micro- and mesoporous regimes. Important factors influencing the structure and dynamics of confined liquids include the average pore size and pore size distribution, the degree of pore interconnection, and the character of the fluid-pore wall interaction.

The properties of supercritical CO_2 inside small pores are of interest for both supercritical fluid chromatography and subsurface carbon storage. Increased levels of CO_2 in the atmosphere, resulting from fossil fuel burning, have a deleterious impact on global climate and the acidity of the oceans. Large-scale CO_2 capture and storage in porous rock formations at 1−3 km depth is seen as one mitigation strategy. In this process, CO_2 is separated from the flue gas, compressed, and pumped into reservoir rocks with overlying caprocks (seals). Metal organic frameworks (MOF's),[2,3] zeolites,[4−7] and chemically modified silica matrices[8] are studied as adsorbents for CO_2 capture. Reservoir rock targets are sandstone, unmineable coal seems, and basalt formations, while suitable caprocks may be formed by thick layers of clay-rich shales or mudstones overlying the reservoir rock.[9,10]

Under storage conditions, CO_2 is a supercritical, buoyant fluid. Depending on the rock properties and operating parameters of the storage site and actual distance to the injection well, CO_2 and brine will occupy the pore spaces in widely varying ratios. For the purposes of site selection, long-term reservoir behavior prediction, and risk assessment, the interactions of supercritical CO_2 with porous solids need to be quantified. Gravimetric or volumetric sorption techniques have assessed the sorption of supercritical CO_2 onto coal and clays as a means of exploring the potential of large-scale storage of anthropogenic CO_2 in geological reservoirs.[11−14] Enhanced coalbed methane production using CO_2 has been studied in ref 15. Carbon sequestration in saline aquifers involves brine displacement, which can

Received: September 27, 2011
Revised: December 2, 2011

 © XXXX American Chemical Society

create dryout zones, accompanied by salt precipitation and changes in porosity and permeability.[16−18] Modeling of these very complex systems is crucial for our understanding but requires detailed knowledge of the individual fluid−fluid and fluid−solid interactions.

High-pressure sorption experiments with engineered porous materials allow for control of pore size and morphology, facilitating data interpretation, and modeling. Near-critical sorption measurements of CO_2 to activated carbon are reported in refs 19−23; supercritical CO_2 in porous silica has been studied in refs 24−29. The molecular interactions of CO_2 with silica surfaces have been reported in refs 30 and 31.

The Controlled Pore Glass (CPG-10) used in this study is synthetic mesoporous silica, which is available in a wide range of pore sizes with narrow size distributions and identical chemical properties and surface morphologies in each sample. Quartz is a major component in some rock types deemed suitable for carbon storage, including sandstone, and while CPG-10 glasses consist of ca. 96% of amorphous SiO_2, they are considered reasonable proxies for hydrophilic rock pore surfaces. Many rocks possess considerable amounts of nanoporosity, often with a fractal distribution of pore sizes.[32−34]

The goal of this study is to study supercritical sorption of CO_2 in mesopores and, to the extent possible, delineate surface and confinement effects. By studying synthetic model systems with well-defined pore size, changes in confined CO_2 properties with pore size can be measured more directly than in natural rock samples with wide pore size distribution. This information can then be used to assess CO_2 behavior in the more complex environments encountered in carbon storage.

2. SORPTION QUANTITIES AND MODELS

Excess sorption is defined as the excess amount of fluid stored in the sorption layer

$$n_e = \int_0^\infty [\rho(z) - \rho_b] dz$$

where $\rho(z)$ is the local fluid density at distance z from the interface, and ρ_b is the bulk fluid density. The excess sorption takes positive values for interfacial fluid enrichment and negative values for fluid depletion at the solid interface but contains no direct information about the interfacial fluid density profile. To obtain this information, the Gibbs surface excess model is often applied in which the (commonly unknown) inhomogeneous fluid density profile is represented by a step profile, i.e., a sorption phase with constant density and composition, separated from the bulk fluid phase by the Gibbs interface.[35,36] Fluid adsorption in porous materials is additionally characterized by the quantity total adsorption, which gives the overall amount of fluid contained in the pore spaces, i.e., it accounts for both the adsorbed and unadsorbed pore fluid. The accuracy of sorption measurements can be limited by uncertainties in the determination of the accessible pore volume, which is most relevant for volumetric measurements.[37]

The sorption of subcritical fluids in narrow pores involves pore condensation in which the pore-confined fluid condenses at a lower pressure than the corresponding bulk fluid. The Kelvin equation relates the pore condensation pressure p, normalized to the bulk condensation pressure p_0, and to the pore radius r

$$RT \ln\left(\frac{p}{p_0}\right)_{pc} = -\frac{\sigma}{\Delta\rho r}$$

Table 1. Characterization of the CPG-10 Materials Used in This Study (Data Provided by Millipore)

material	mean pore diameter (Å)	pore size distribution (±%)	pore volume V_p (cm^3/g)	specific surface area S_A (m^2/g)	particle size range (mm)
CPG75C	81	8.9	0.49	197	0.2−0.4
CPG350C	318	4.0	0.97	70.5	0.2−0.4

In this equation, R is the universal gas constant, T is the temperature, σ is the surface tension of bulk liquid, and $\Delta\rho$ is the density difference between liquid and gas. For small pores, the Kelvin equation is known to underestimate the pore size calculated from the observed shift in the pore condensation pressure.[38] Several explanations exist for this behavior. Cohan proposed the formation of thin adsorbed fluid layers before the onset of pore condensation, which effectively reduce the pore size at pore condensation.[39] Another modification to the Kelvin equation, accounting for the nanoscale structure of the fluid−gas interface, is discussed by Digilov.[40] While these models account for the molecular-scale structures of the pore-confined fluid, a separate matrix-response effect has recently been studied intensively.[41−44] The impacts of pore size and morphology, temperature, and fluid−substrate combinations on pore condensation are discussed in refs 45−47.

Pore condensation vanishes above the critical point of the pore fluid, which is usually shifted to lower temperatures with respect to the critical point of the bulk fluid. While some of the mechanisms found in subcritical fluid sorption are expected to extend into the supercritical region, true phase nanoscale separation between the adsorbed and unadsorbed fluid phases does not occur under supercritical conditions. Measurements at subcritical temperatures commonly cover only low bulk fluid densities, i.e., adsorption from the gas or vapor phase, because at higher densities the vapor−liquid coexistence curve is intersected. For supercritical fluids, this limitation disappears. However, relatively fewer experimental data are available on supercritical as compared to subcritical sorption, and the impacts of pressure and temperature conditions, molecular fluid−solid interactions, pore size, and morphology on supercritical sorption processes are still partially unexplored.

At temperatures above the pore critical point, gradual pore filling through multilayer adsorption replaces the instantaneous process of pore condensation, and disappearance of sorption hysteresis is observed. Molecular dynamics simulation of supercritical fluid adsorption indicates that fluid density perturbations near surfaces can extend several tens of molecular diameters into the subphase or pore space.[48] Fluids in cylindrical and slit pores were also studied with density functional theory.[49,50] In these studies, a shift of the maximum in the excess sorption to higher bulk fluid density with increasing pore width was found, although no detailed explanation was provided.

3. MATERIALS AND EXPERIMENTAL METHOD

Two CPG-10 silica materials, purchased from Millipore, with nominal pore sizes of 7.5 nm (CPG75C, Lot No 01C009) and 35 nm (CPG350C, Lot No J7SN05C027) were selected for this study. A summary of their physical properties, provided by the manufacturer, is given in Table 1 and a SEM photomicrograph is presented in Figure 1. Pore volume and specific surface area of CPG75C were measured by N_2-BET in our laboratories, and very good agreement with the data provided by the manufacturer

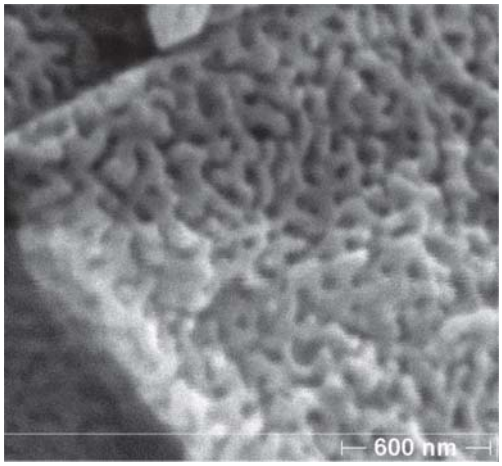

Figure 1. Raster electron microscopic images of CPG-10 with 500 Å nominal pore size, showing the wormlike and interconnected structure of the nanopores.

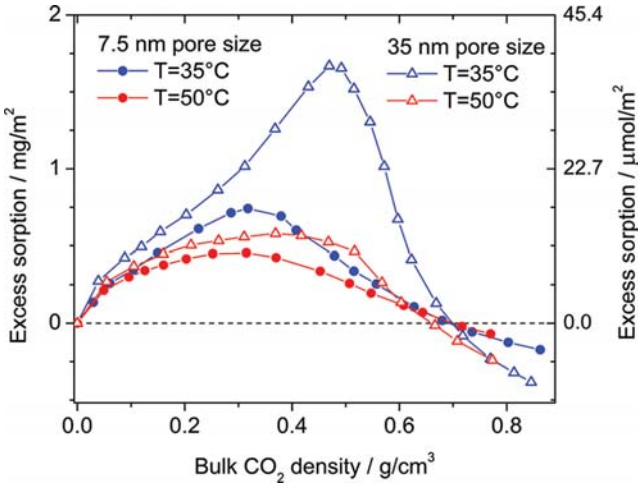

Figure 2. Excess sorption of supercritical CO_2 in CPG-10 materials, normalized to the specific surface area.

was obtained. Both materials have pore networks comprised of interconnected pores with local cylindrical shape and relatively uniform pore width. From these data, the porosities of CPG75C and CPG350C were calculated to be 52% and 68%, respectively. The hydraulic pore radii, calculated by $r_h = 2V_p/S_A$, with V_p the pore volume and S_A the specific surface area, are 5 nm for CPG75C and 27 nm for CPG350C. These values are larger than the nominal pore sizes given in Table 1. The skeletal density of CPG-10 was measured with contrast-variation small-angle neutron scattering (SANS), yielding a value of 2.2 g/cm^3.[51] This value is, as expected for amorphous silica, lower than the density of α-quartz (2.65 g/cm^3) but close to the density of cristobalite (2.33 g/cm^3).

A Rubotherm high-pressure gravimetric sorption apparatus at the DEGAS laboratories at the Helmholtz Center Berlin, Germany, was utilized in this study. Temperature was measured with a calibrated Pt-100 temperature sensor mounted directly underneath the sample bucket. The temperature was held within ±20 mK by electrical resistance heaters wrapped around the outside of the pressure vessel and controlled by a PID type programmable controller unit. Temperature equilibrium was achieved within 20−30 min after a change in fluid pressure or temperature. The large uncertainties in the excess sorption measurement reported in ref 52 due to poor temperature control were avoided here by use of an electrical heater coil, ensuring good temperature stability throughout the pressure measurement cell. Furthermore, we did not study the near-critical region, i.e., temperatures within $T_c \pm 1$ K, where thermostat errors would have the greatest effect.

The fluid pressure in the cell was measured with a Keller Preciseline transducer with a range of 0−300 bar and calibrated accuracy of better than 0.01% full scale, i.e., ± 0.03 bar. The suspension balance has a stated resolution of ±0.01 mg and a reproducibility of ±0.02 mg.

To perform a sorption experiment, 200−300 mg of the adsorbent were weighed into the sample bucket using a microbalance with 0.01 mg accuracy. The filled sample bucket was then inserted into the sorption apparatus, and the sample and measurement chambers were evacuated at an elevated temperature (T = 50 °C) using a two-stage turbo-molecular pump until sample weight constancy was achieved, i.e., for 1−3 h. This procedure ensured that water and volatile organics initially present in the pore spaces are removed, while the surface remained hydroxylated. Carbon dioxide with a purity of 99.999%, purchased from Linde AG, Germany, was transferred into a piston pressure generator cooled to 10 °C. The fluid was introduced into the measurement cell in small amounts through a needle valve. Measurements were performed by admitting the desired amount of fluid into the cell and closing the inlet valve. Continuous measurements of temperature, pressure, and sample weight were performed until thermal, pressure, and sample weight constancy were achieved. At equilibrium, fluctuations in the temperature were ±20 mK, pressure stability was on the order of ±0.05 bar, and the sample weight stability was ±10 μg. Typical equilibration times were on the order of 0.5−1 h per data point. Sorption equilibrium was assumed when all parameters remained constant over at least 15 min. The fluid pressures at sorption equilibrium were converted to fluid densities using the REFPROP 9 software from NIST.[53] This software, for pure CO_2, uses the equation of state (EOS) provided by Span and Wagner.[54] The excellent accuracy of this EOS has been recently confirmed by vibrating tube densimetry measurements carried out over a wide range of pressure and temperature.[55] The data were corrected for the buoyancy effects resulting from immersing the sample bucket and connecting rods in the measurement fluid and apparatus. Corrections were also made for the adsorbent buoyancy, using a SiO_2 skeletal density of 2.2 g/cm^3. Experimental errors in the bulk density and excess sorption data are within the size of the data points shown on the figures.

4. RESULTS AND DISCUSSION

Excess sorption isotherms for both CPG-10 materials were measured at two temperatures and normalized to both the specific surface area and the pore volume using the data given in Table 1. Additionally, mean pore density, a quantity closely related to total adsorption, is considered. Results are plotted as a function of bulk fluid density, ρ_b, to simplify comparison of sorption data measured at different temperatures.

4.1. Surface Area Normalized Excess Sorption. Excess sorption isotherms, normalized to the specific surface area (Table 1), are shown in Figure 2. All isotherms show similar general behavior, i.e., initial increase of excess sorption, then formation of broad excess sorption maxima, followed by steady

and gradual decreases of the excess sorption with increasing bulk densities. At low bulk fluid densities, i.e., $\rho_b < 0.1$ g/cm^3, the isotherms show similar behavior, i.e., small pore size and weak inverse temperature dependences. However, in the region $0.1 < \rho_b$/g/cm$^3 < 0.7$, effects of pore size and temperature become more pronounced.

A number of differences in the sorption behaviors of the two chemically identical matrices with different pore sizes suggest that the confinement affects the manner in which CO_2 is adsorbed. The excess sorption peak position shifts from $\rho_b \approx 0.3$ g/cm^3 for CPG75C to $\rho_b \approx 0.45$ g/cm^3 for CPG350C. Both values are smaller than the bulk critical density of CO_2, $\rho_c = 0.4676$ g/cm^3.[54] Such a shift in the excess sorption maximum was qualitatively predicted from computer simulations of supercritical fluid adsorption in narrow cylindrical[49] and slit pores.[56] In simulation studies, the pore sizes are often expressed in molecular dimensions. To compare these simulation results with our experimental data, a spherical diameter of about 4.1 Å for the CO_2 molecule is assumed, which yields pore sizes of ~20 molecular diameters for CPG75C and ~80 molecular diameters for CPG350C. The pore sizes studied in ref 49 fall in this range, while the pores investigated in ref 56 are narrower. Thus, the position of the excess sorption maximum appears to be controlled by the strength of geometrical confinement or pore wall curvature, i.e., at a given pressure a denser sorption phase is stabilized in the smaller pores. No temperature dependence of the excess sorption maximum position is observed, i.e., an excess sorption maximum shift to lower fluid densities with decreasing temperature, as was predicted from these simulations, is small or not present here. This effect may be, however, subdued by the small temperature range studied.

An increase in the maximum of the excess sorption isotherm with decreasing temperature was found for both pore widths but is more pronounced for the material with the wider pores. At $T = 35$ °C, the maximum of the S_A-normalized surface excess in the wider pores is more than three times larger than in the narrow pores. The effect is weaker at $T = 50$ °C and indicates that the interfacial fluid density profile is distorted by the spatial confinement, at least in the narrower pores. Since the formation of the interfacial fluid layer is more spatially restricted in the narrower pores, hence the smaller S_A-normalized surface excess.

At high fluid density, i.e., $\rho_b \approx 0.65-0.7$ g/cm^3, all sorption isotherms show a point of zero excess sorption, i.e., a regime consisting of identical densities for the sorption phase and the bulk phase, and/or a vanishingly small volume of the sorption phase. The relative independence of the sorption properties on the pore size may indicate a dominating influence of adsorbate–surface interactions in this region, analogous to the fluid behavior at $\rho_b < 0.1$ g/cm^3. Further increase in fluid density gives rise to negative values of excess sorption, implying formation of an interfacial fluid layer with reduced density or fluid packing inefficiencies in the pore spaces. The pressure range of our experimental setup did not permit assessment of the sorption properties at pressures above 200 bar, which could provide a better understanding of this behavior.

4.2. Excess Sorption Normalized to Pore Volume. The surface area normalized excess sorption data indicate confinement effects, possibly by limiting the thickness of the sorption layer in nanopores. Multilayer adsorption in narrow pores may exhibit confinement effects when sorption layers formed at opposing pore walls begin to overlap in the pore center, impeding further growth in thickness of the sorption layers. In this case, the surface area normalized excess sorption should increase with increasing pore size. However, the density profiles formed in narrower pores should contain larger fractions of near-surface fluid with higher density. Normalizing the excess sorption to the pore volume (listed in Table 1) and comparing the pore volume normalized excess sorption data to the surface area normalized excess sorption data can test this hypothesis. In Figure 3, the pore volume normalized excess sorption is shown as a function of the bulk fluid density.

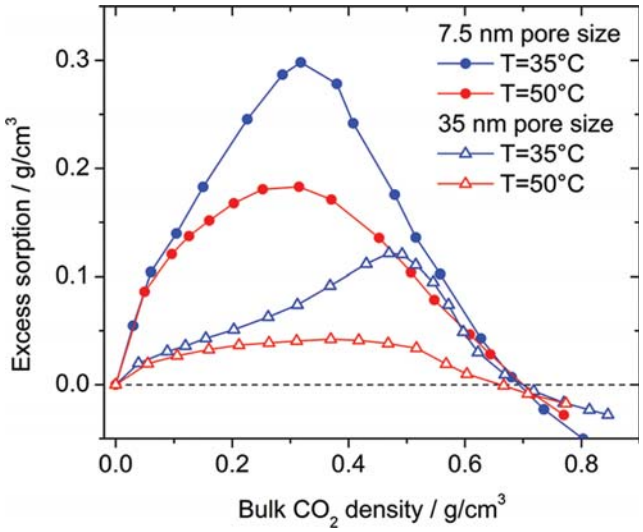

Figure 3. Excess sorption of supercritical CO_2 in CPG-10, normalized to the pore volume.

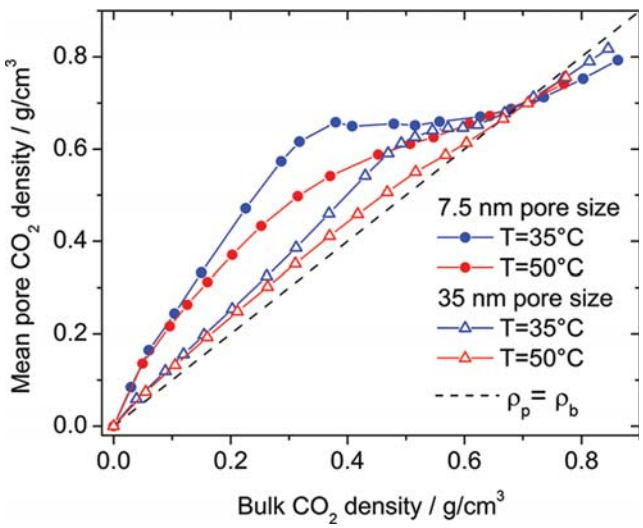

Figure 4. Mean pore density of supercritical CO_2 in CPG-10. The dashed line visualizes the hypothetical case of zero sorption.

At low fluid densities (i.e., $\rho_b < 0.3$ g/cm^3), excess sorption increases more rapidly and is up to 4 times higher in the smaller pores compared to that in the larger pores. The pore-size normalized data show less pronounced adsorption at low ($\rho_b < 0.1$ g/cm^3) and less pronounced depletion at high bulk density ($\rho_b < 0.7$ g/cm^3) in the larger pores.

4.3. Mean Density of Pore Fluid. The mean density of pore fluid, ρ_p, is readily calculated from the pore volume normalized

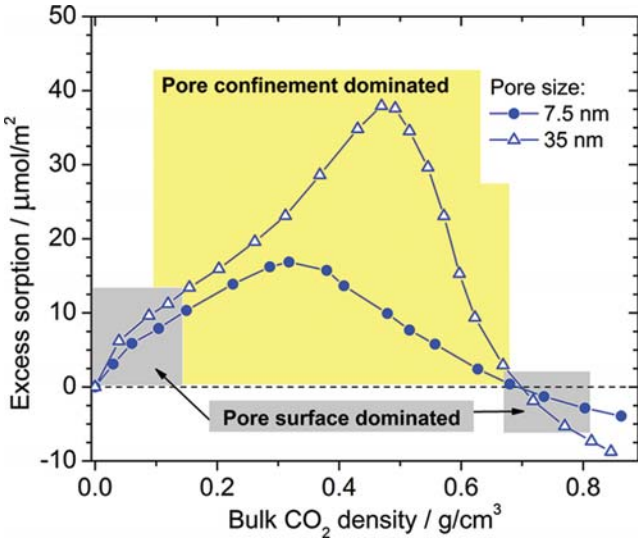

Figure 5. Sorption isotherms at T = 35 °C, normalized to the specific surface area. Sections of the isotherms in which the fluid−pore surface interactions appears to dominate are highlighted in gray. The region of strong confinement effects is highlighted in yellow.

excess sorption data by $\rho_p = \rho_b + \rho_e$, with ρ_e being the excess density of pore fluid. The results, given in Figure 4, show a higher CO_2 mean pore density in the smaller pores for $\rho_b < 0.6$ g/cm^3. Notably, the 35 °C isotherms show regions of constant pore density for both pore widths. For the smaller pores, the constant pore density plateau covers $0.35 \leq \rho_b$/g/cm$^3 \leq 0.6$, while it extends from $0.5 \leq \rho_b$/g/cm$^3 \leq 0.6$ in the larger pores. The pore fluid densities in the plateau region are similar, i.e., values of $\rho_p \approx 0.65$ g/cm^3 are measured for both pore widths. From Figures 3 and 4, it can be seen that the maximum of the excess sorption curve and the onset of constant mean pore density occur at approximately the same bulk fluid density. The pore densities again increase at $\rho_b > 0.6$ g/cm^3 but with shallower slopes.

At T = 50 °C, no regions of constant pore density are observed; however, the same crossover to pore depletion is observed at high density (i.e., the mean pore fluid is less dense than the bulk fluid). Brovchenko and Oleinikova showed with molecular dynamics simulations of Leonard-Jones fluids near solid interfaces and in nanopores that, for weakly attractive solid−fluid interaction potentials, interfacial fluid depletion occurs at high bulk fluid density.[57,48] They ascribed this behavior to the combined effects of the surface field imposed by the solid and the missing neighbor effect of fluid molecules in the interfacial layer.

5. CONCLUSIONS

Nanoscale pore confinement effects on the properties of supercritical CO_2 were studied by means of excess sorption measurements. Pores with sizes on the length scale of tens of nanometers impact fluid sorption properties over wide ranges of bulk fluid densities, most prominently in the region of strong adsorption. A pronounced shift of the maximum excess sorption to higher bulk fluid densities with increasing pore size was found. This dependence is similar to the change in pore condensation pressure with pore size although it is unlikely that a sharp adsorbed phase−bulk fluid interface is formed under supercritical conditions. The silica pore surface presented by CPG-10 might be characterized as weakly attractive for supercritical CO_2, i.e., the fluid adsorbs to the surface only at fluid densities $\rho_b < 0.7$ g/cm^3. In the strong adsorption region, fluid sorption in the narrow and possibly also the wider pores is limited by the spatial confinement. However, adsorption at both low and high bulk density appears to be controlled by surface−fluid interactions. This tentative model is summarized, illustrated by the sorption data taken at the lower temperature, in Figure 5.

Results from this study may be applied to assess the storage capacity of CO_2 in quartz-rich geological formations such as sandstones. Because different lithologic units are likely to be buried to different depths and temperatures and to have different average pore widths, our results suggest that these units will also have different storage capacities. The CO_2 storage capacity will be higher for sites that are shallower and/or are in areas of low geothermal gradient and therefore have lower temperatures. The CO_2 storage capacity will also be greater in rocks characterized by a large fraction of narrow (small) pores with high surface to volume ratios. In fine-grained quartz sandstone formations or sandstones with greater nanoporosity due to quartz overgrowths [L. M. Anovitz et al., in review], a significant densification of CO_2 in the pores can be expected, while in larger pores, CO_2 can be stored with near-bulk density. The increased density of CO_2 in rocks with smaller pores means that a larger mass of CO_2 can be stored in a smaller volume of rock, compared to rocks with larger average pore size.

AUTHOR INFORMATION

Corresponding Author
*E-mail: rotherg@ornl.gov.

ACKNOWLEDGMENT

This material is based upon work supported as part of the Center for Nanoscale Control of Geologic CO_2, an Energy Frontier Research Center funded by the U.S. Department of Energy, Office of Science, Office of Basic Energy Sciences. E.G.K. and R.J.B. were supported through the NETL-Regional University Alliance (NETL-RUA) in support of the National Energy Technology Laboratory's ongoing research in carbon sequestration under the RES Contract DE-FE0004000. We are thankful for the comments from Dr. Andreas Busch and two anonymous reviewers.

REFERENCES

(1) Gelb, L. D.; Gubbins, K. E.; Radhakrishnan, R.; Sliwinska-Bartkowiak, M. *Rep. Prog. Phys.* **1999**, *62* (12), 1573.
(2) Lastoskie, C. *Science* **2010**, *330*, 595.
(3) Salles, F.; Jobic, H.; Devic, T.; Llewellyn, P. L.; Serre, C.; Férey, G.; Maurin, G. *ACS Nano* **2010**, *4*, 143.
(4) Liu, S.; Yang, X. *J. Chem. Phys.* **2006**, *124*, 244705.
(5) Pini, R.; Ottiger, S.; Rajendran, A.; Storti, G.; Mazzotti, M. *Adsorption* **2008**, *14*, 133.
(6) Krishna, R.; Van Baten, J. M. *Langmuir* **2009**, *26*, 3981.
(7) Cole, D. R.; Chialvo, A. A.; Rother, G.; Vlcek, L.; Cummings, P. T. *Philos. Mag.* **2010**, *90*, 2339.
(8) Zeleňák, V.; Badaničová, M.; Halamová, D.; Čejka, J.; Zukal, A.; Murafa, N.; Goerigk, G. *Chem. Eng. J.* **2008**, *144*, 336.
(9) Benson, S. M.; Cole, D. R. *Elements* **2008**, *4*, 325.
(10) Cole, D. R.; Mamontov, E.; Rother, G. In *Neutron Applications in Earth, Energy, and Environmental Sciences*; Liang, L., Rindaldi, R., Schober, H., Eds.; Springer Verlag: Berlin, Germany, 2009; pp 547−570.
(11) Jwayyed, A. M.; Humayun, R.; Tomasko, D. L. *Rev. Sci. Instrum.* **1997**, *68*, 4542.

(12) Busch, A.; Krooss, B. M.; Gensterblum, Y.; Van Bergen, F.; Pagnier, H. J. M. *J. Geochem. Explor.* **2003**, *78*−*79*, 671.
(13) Busch, A.; Alles, S.; Gensterblum, Y.; Prinz, D.; Dewhurst, D. N.; Raven, M. D.; Stanjek, H.; Kroos, B. M. *Int. J. Greenhouse Gas Control* **2008**, *2*, 297.
(14) Gensterblum, Y.; Van Hemert, P.; Billemont, P.; Busch, A.; Charriére, D.; Li, D.; Krooss, B. M.; De Weireld, G.; Prinz, D.; Wolf, K.-H. A. A. *Carbon* **2009**, *47*, 2958.
(15) Gruszkiewicz, M. S.; Naney, M. T.; Blencoe, J. G.; Cole, D. R.; Pashin, J. C.; Carroll, R. E. *Int. J. Coal Geol.* **2009**, *77*, 23.
(16) Perrin, J.-C.; Benson, S. *Transp. Porous Media* **2010**, *82*, 93.
(17) Muller, N.; Qi, R.; Mackie, E.; Pruess, K.; Blunt, M. J. *Energy Procedia* **2009**, 3507.
(18) Ott, H.; de Kloe, K.; Marcelis, F.; Makurat, A. *Energy Procedia* **2011**, 4425.
(19) Chen, J. H.; Wong, D. S. H.; Tan, C. S.; Subramanian, C. T.; Lira, C. T.; Orth, M. *Ind. Eng. Chem. Res.* **1997**, *36*, 2808.
(20) Humayun, R.; Tomasko, D. L. *AIChE J.* **2000**, *46* (10), 2065.
(21) Zhou, L.; Zhou, Y.; Bai, S.; Yang, B. *Adsorption* **2002**, *8*, 125.
(22) Zhou, L.; Bai, S.; Su, W. *Langmuir* **2003**, *19*, 2683.
(23) Do, D. D.; Do, H. D. *J. Chem. Phys.* **2005**, *123*, 084701.
(24) Zhou, L.; Zhou, Y.; Bai, S.; Yang, B. *J. Colloid Interface Sci.* **2002**, *253*, 9.
(25) Tatsuda, N.; Goto, Y.; Setoyama, N.; Fukushima, Y. *Adsorpt. Sci. Technol.* **2005**, *23*, 763.
(26) Steriotis, Th. A.; Stefanopoulos, K. L.; Katsaros, F. K.; Gläser, R.; Hannon, A. C.; Ramsay, J. D. F. *Phys. Rev. B* **2008**, *78*, 115424.
(27) Belmabkhout, Y.; Serna-Guerrero, R.; Sayari, A. *Chem. Eng. Sci.* **2009**, *64*, 3721.
(28) Omi, H.; Ueda, T.; Miyakubo, E. *Appl. Surf. Sci.* **2005**, *252*, 660.
(29) Melnichenko, Y. B.; Mayama, H.; Cheng, G.; Blach, T. *Langmuir* **2010**, *26*, 6374.
(30) Vishnyakov, A.; Shen, Y.; Tomassone, M. S. *J. Chem. Phys.* **2008**, *129*, 174704.
(31) Roque-Malherbe, R.; Polanco-Estrella, R.; Marquez-Linares, F. *J. Phys. Chem. C* **2010**, *114*, 17773.
(32) Radlinski, A. P.; Radlinska, E. Z.; Agamalian, M.; Wignall, G. D.; Lindner, P.; Randl, O. G. *Phys. Rev. Lett.* **1999**, *82*, 3078.
(33) Anovitz, L. M.; Lynn, G. W.; Cole, D. R.; Rother, G.; Allard, L. F.; Hamilton, W. A.; Porcar, L.; Kim, M.-H. *Geochim. Cosmochim. Acta* **2009**, *73*, 7303.
(34) Jin, L.; Rother, G.; Cole, D. R.; Mildner, D. F. R.; Duffy, C. J.; Brantley, S. L. *Am. Mineral.* **2011**, *96*, 498.
(35) Gibbs, J. W. *The Collected Works of J. Williard Gibbs*; Longmans: Green, NY, 1928; Vol. 1, p 219.
(36) Sircar, S. *Ind. Eng. Chem. Res.* **1999**, *38*, 3670.
(37) Do, D. D.; Do, H. D.; Fan, C.; Nicholson, D. *Langmuir* **2010**, *26*, 4796.
(38) Llewellyn, P. L.; Rouquerol, F.; Rouquerol, J.; Sing, K. S. W. *Characterization of Porous Solids V*, Studies in Surface Science and Catalysis; Elsevier: New York, 2000; Vol. 128, p 421.
(39) Cohan, L. H. *J. Am. Chem. Soc.* **1944**, *66*, 98.
(40) Digilov, R. *Langmuir* **2000**, *16*, 1424.
(41) Zickler, G. A.; Jähnert, S.; Funari, S. S.; Findenegg, G. H.; Paris, O. *J. Appl. Crystallogr.* **2007**, *40*, s522.
(42) Günther, G.; Prass, J.; Paris, O.; Schoen, M. *Phys. Rev. Lett.* **2008**, *101*, 086104.
(43) Schoen, M.; Paris, O.; Günther, G.; Müter, D.; Prass, J.; Fratzl, P. *Phys. Chem. Chem. Phys.* **2010**, *12*, 11267.
(44) Gor, G. Yu.; Neimark, A. V. *Langmuir* **2011**, *27*, 6926.
(45) Thommes, M.; Köhn, R.; Fröba, M. *J. Phys. Chem. B* **2000**, *104*, 7932.
(46) Schreiber, A.; Bock, H.; Schoen, M.; Findenegg, G. H. *Mol. Phys.* **2002**, *100*, 2097.
(47) Mascotto, S.; Wallacher, D.; Brandt, A.; Hauss, T.; Thommes, M.; Zickler, G. A.; Funari, S. S.; Timmann, A.; Smarsly, B. M. *Langmuir* **2009**, *25*, 12670.
(48) Oleinikova, A.; Brovchenko, I. *Phys. Rev. E* **2008**, *78*, 061601.
(49) Evans, R.; Marini Bettolo Marconi, U. *J. Chem. Soc., Faraday Trans.* **1986**, *2*, 1763.
(50) Evans, R.; Marini Bettolo Marconi, U.; Tarazona, P. *J. Chem. Phys.* **1986**, *84*, 2376.
(51) Schemmel, S.; Rother, G.; Eckerlebe, H.; Findenegg, G. H. *J. Chem. Phys.* **2005**, *122*, 244718.
(52) Pini, R.; Ottiger, S.; Rajendran, A.; Storti, G.; Mazzotti, M. *Adsorption* **2006**, *12*, 393.
(53) Lemmon, E. W.; Huber, M. L.; McLinden, M. O. *NIST Standard Reference Database 23: Reference Fluid Thermodynamic and Transport Properties*, version 9.0; National Institute of Standards and Technology: Gaithersburg, MD, 2010.
(54) Span, R.; Wagner, W. *J. Phys. Chem. Ref. Data* **1996**, *25*, 1509.
(55) Velasco, I.; Rivas, C.; Martínez-López, J.; Blanco, S. T.; Otín, S.; Artal, M. *J. Phys. Chem. B* **2011**, *115*, 8216.
(56) Van Megen, W.; Snook, I. K. *Mol. Phys.* **1985**, *3*, 741.
(57) Oleinikova, A.; Brovchenko, I.; Geiger, A. *Eur. Phys. J. B* **2006**, *52*, 507.